中國機械工程學刊第三十九卷第六期第 599~608 頁(民國一百零七年)
Journal of the Chinese Society of Mechanical Engineers, Vol.39, No.6, pp 599~608 (2018)

Design and Analysis of Suspension System Based on Tire Characteristics

Zhi-Qiang Liang**, Xin-Tian Liu*, He Zuo** and Yan-Song Wang*

Keywords：suspension system, tire characteristics, multi-body dynamics, geometric parameters, alignment parameters

ABSTRACT

Suspension system is the key component of vehicle for riding comfort and stability. This paper describes how to design and analyse the suspension system. According to the tire characteristics, geometric parameters of the transverse arms, elastic elements and damping elements are firstly determined. Then the dynamic model of the vehicle suspension system is established. Finally, the kinematic and dynamic analysis are carried out to verify the effectiveness of the suspension system design. According to the analysis results, the benefits of the design method is evident.

INTRODUCTION

When designing the vehicle, contemporary tuning of tire characteristics and suspension system is of crucial importance (Mastinu et al. 2006). In particular, the suspension system plays an important role in the handing stability and riding comfort (Balamurugan et al. 2014). And the suspension design is a compromise between the vehicle's comfort level and handing (Eskandary et al. 2016). Therefore, in this paper, the design of suspension system based on tire characteristics are carried out. Then both kinematic and dynamic analysis of the designed suspension system are performed (Hunrel et al. 2013).

Typical independent suspensions include double wishbone type and Macpherson strut type (Kim et al. 2012). By considering space and placement, the double wishbone suspension is chosen for vehicle (Liu et al. 2015). The suspension design is decided by the several suspension characteristics (camber, toe, caster, wheel base, wheel track). Recently, the design and optimization of suspension system have been studied (Angrosch et al. 2014). A robust suspension optimization is presented with considering bush compliance uncertainty (Kang et al. 2010). The design process of the vehicle suspension is introduced, including the determination of geometric parameters, spring stiffness and damping coefficient. Park and Sohn (2012) studied the effects of camber angle control on vehicle dynamic behaviors. Reimpell et al. (2001) made a detailed introduction to the suspension kinematics and analyzed its influence on the vehicle handing stability. Wolfgang (1998) also studied the kinematics and dynamics of suspension system deeply. Uchida and Mcphee (2012) formulated the equations of motion for a double-wishbone suspension using linear graph theory. And the lateral kinematics of the vehicle suspension system based on C0rrevitS-400 sensor is analyzed in detail (Stéphant et al. 2007). In addition, the multi-objective optimization by compressively considering various factors that affect vehicle handing is carried out (Jamali et al. 2014).

This paper mainly discusses the design and analysis of suspension system based on tire characteristics. This paper is organized as follows. In section 1, tire characteristics are mainly discussed, including the side-slip characteristics, aligning torque and slip ratio. In section 2, the geometric parameters of front and rear suspension transverse arms are determined. In section 3, the stiffness of elastic elements and the damping coefficient of damping elements are calculated. In section 4, the dynamic model of the vehicle suspension system is established, then the kinematic and dynamic analysis are carried out. Finally, in section 5, the conclusions are summarized.

TIRE CHARACTERISTICS

Tire is one of the most important components of the vehicle. It is the determinant of vehicle handing stability and braking performance. In this

Paper Received November, 2016. Revised September, 2018, Accepted September, 2018, Author for Correspondence: Xin-Tian Liu.

* *Professor, School of Mechanical and Automotive Engineering, Shanghai University of Engineering Science, Shanghai 201620, China.*

** *Gradnate Student, School of Mechanical and Automotive Engineering, Shanghai University of Engineering Science, Shanghai 201620, China.*

section, the Pacejka 2002 tire model is used to fit the original tire test data and the results are obtained. Then tire characteristics are analyzed, which provides a basis for the suspension design. The SAE J670 standard (Pacejka 2002) is adopted to establish the tire moving coordinate system and study the tire characteristics.

Side-Slip Characteristics

The lateral force-sideslip angle curve of the tire is shown in Figure.1. The curve shows that the change of lateral force along with side-slip angle can be divided into three stages-linear, transition and friction. In linear phase, side-slip angle is small. The relationship between lateral force and side-slip angle is linear and the slope is called tire cornering stiffness. In transition phase, the slope of the curve gradually decreases. When the slope is equal to zero, the maximum lateral force of the tire is reached. With the increase of side-slip angle, the lateral force begins to decrease, and lateral sliding between the tire and ground appears obviously.

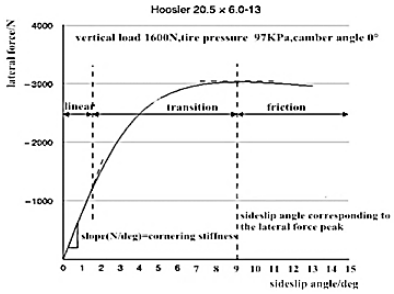

Fig.1. Lateral force-sideslip angle curve

The cornering stiffness coefficient-vertical load curve of the tire is shown in Figure.2. The product of cornering stiffness coefficient and vertical load is called cornering stiffness. As shown in Fig.2, with the increase of vertical load, the cornering stiffness coefficient decreases gradually. In the process of the vertical load increasing from 100N to 1000N, the cornering stiffness coefficient decreases from 1.19 to 0.75. The greater the vertical load, the smaller the cornering stiffness coefficient.

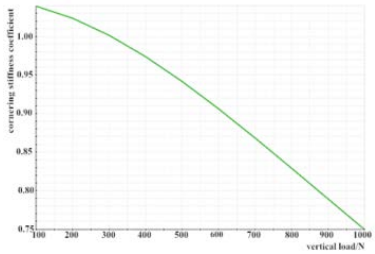

Fig. 2. Cornering stiffness coefficient-vertical load

The lateral adhesion coefficient-vertical load curve of the tire is shown in Figure. 3. The ratio of the peak lateral force and the vertical load is called lateral adhesion coefficient. As shown in Fig. 3, with the increase of vertical load, the lateral adhesion coefficient decreases. The lower the vertical load, the higher the lateral adhesion coefficient, and the better the side-slip characteristic of the tire.

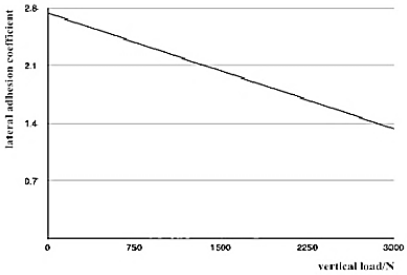

Fig.3. Lateral adhesion coefficient-vertical load

The lateral force-sideslip angle curves of the tire corresponding to different camber angles are shown in Figure.4. The curves A, B, C, D and E respectively correspond to different working conditions of camber angles of 0 degrees, 1 degrees, 2 degrees, 3 degrees and 4 degrees. As shown in Fig.4, when the camber angle is 0 degrees, the curve passes through the coordinate origin and the peak lateral force is the largest. With the increase of the tire camber angle, the linear interval of the curve shifts upward but the cornering stiffness remains constant, and the slope gradually decreases in transition interval. When the side-slip angle is equal to 3.7 degrees, the curves intersect at one point. In addition, when the side-slip angle is small, moderate camber angle will increase the value of lateral force, but will decrease the peak value of lateral force.

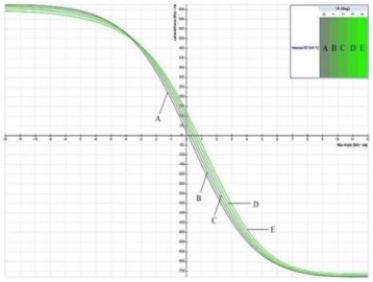

Fig. 4. The lateral force-sideslip angle curve

When calculating the offset frequency of suspension, the change of tire pressure will have a significant impact on the vertical stiffness. The steering characteristic of the vehicle can be modified by adjusting the front and rear tire pressure. The peak lateral force-vertical load curve of the tire is shown in Figure.5. The curves A, B, C and D respectively correspond to different working conditions of tire pressure of 8 psi, 10 psi, 12 psi and 14 psi. When the vertical load ranges from 100N to 1150N, the lower the tire pressure, the higher the peak lateral force. However, when the vertical load is greater than 1500N, the higher the tire pressure, the higher the peak lateral force. Because the lower tire pressure leads to the uneven distributed vertical load of the ground, the tire characteristics become poor. It is concluded that the

tire pressure has a significant impact on the steering characteristic and limit conditions, and the tire pressure needs to be determined based on using conditions.

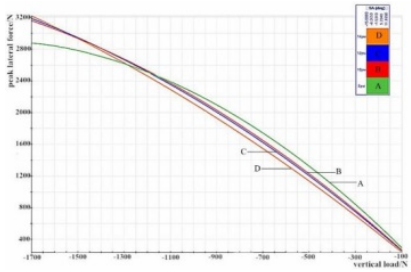

Fig. 5. The peak lateral force-vertical load curve

Aligning Torque

According to the SAE tire coordinate system, the axle of the aligning torque is perpendicular to the ground and passes through the tire-ground point. The aligning torque-sideslip angle curve and the lateral force-sideslip angle curve under this condition are respectively shown in Figure. 6 and Figure. 7.

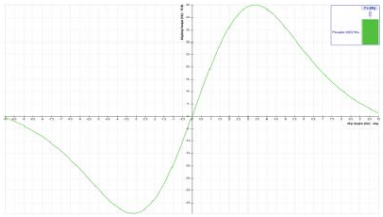

Fig. 6. The aligning torque-sideslip angle curve

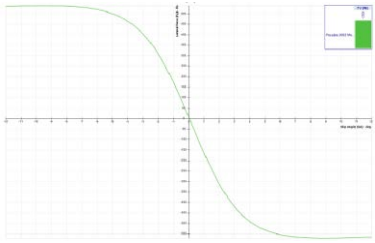

Fig. 7. The lateral force-sideslip angle curve

As can be seen from these figures, not considering the kingpin trail, when the side-slip angle is small (from 0 degrees to 3 degrees), aligning torque and side-slip angle, lateral force and side-slip angle basically follow the linear relationship. With the side-slip angle increasing to 3.5 degrees, the aligning torque reaches maximum value, the lateral force continues to increase and the curve enters into transition interval. Subsequently, the aligning torque decreases gradually. When the side-slip angle is equal to 8.5 degrees, the aligning torque has serious attenuation but the lateral force reaches its peak. With the increase of side-slip angle, the aligning torque decreases to zero or even negative, the lateral force decreases, and lateral sliding between the tire and ground appears obviously. The great significance of the aligning torque lies in the fact that not considering the kingpin trail, with the increase of side-slip angle, the aligning torque has experienced a process from small to great and then to small. The working condition of the tire can be fed back to the driver through the steering wheel, and the driver can get a full warning before the sliding between the tire and ground appears obviously.

Slip Ratio

Similar to the mechanism of lateral force and side-slip angle, the longitudinal force also causes the deformation of the tire, therefore, there will exist relative sliding in the contact area between the tire and the ground. When the vertical load is 1400N, the longitudinal force-slip ratio curve of the tire is shown in Figure.8. Similar to the side-slip condition, the curve also can be divided into three stages-linear, transition and friction. When the slip ratio is greater than zero, the tire is subjected to the driving torque. When the slip ratio ranges from 0% to 2%, the relationship between the longitudinal force and the slip ratio is linear, then the slope of the curve gradually decreases. When the slip ratio is 11%, the longitudinal force reaches its peak value, and then gradually decreases.

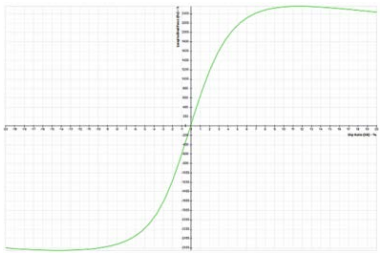

Fig. 8. The longitudinal force-slip ratio curve

Composite Working Condition

The composite working condition of the tire subjected to the longitudinal force and the lateral force at the same time is shown in Figure. 9, which is called the friction circle of the tire. The curves from top to bottom respectively correspond to different working conditions of side-slip angles from -12 degree to 10.737 degree. Each curve respectively corresponds to the relationship between lateral force and longitudinal force under a certain side-slip angle.

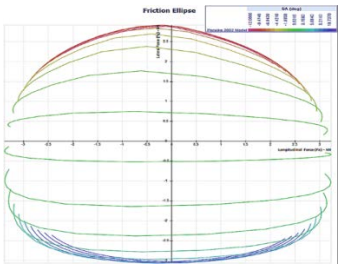

Fig. 9. The friction circle of the tire

As can be seen from Fig. 9, the longitudinal force corresponding to the maximum lateral force is not zero under a certain side-slip angle. This is due to the fact that the deformation of the tire and the increase

of the structural stiffness cause the change of forces of contact area. When the absolute value of the longitudinal force is greater, lateral force obviously decreases, this is due to the friction limit of the tire.

SUSPENSION SYSTEM DESIGN

Determination of Vehicle Basic Parameters

The vehicle's basic parameters should be determined firstly before the suspension geometric design. According to the existing component index and the previous vehicle's parameters, the basic parameters of racing car are shown in Table 1.

Table 1. Basic parameters of vehicle

Item	Size and Specification
Total length/Width/Height	2100mm/1210mm/1140mm
Wheel base	1575mm
Wheel track(F/R)	1210mm/1117mm
Gross weight(F/R)（including a 60kg driver）	145kg/ 155kg
Suspension form	Double-wishbone independent suspension
Tire size and formula	F:20.5x6.0-13 R25B Hoosier R:20.5x7.0-13 R25B Hoosier
Rim width and structure	Width:7 ins, Offset:22mm, Diameter:13 ins
Centroid design height	Height above ground:250mm
Suspension design travel	Compression:25.4mm /Stretching25.4mm
Front caster angle/Pneumatic trail	4 degrees/5mm
Front kingpin inclination angle/Scrub radius	0 degrees/40mm
Anti-dive/Anti-squat/Anti-lift	0%
Static roll center(F/R)	0mm/25.4mm

Determination of Geometric Parameters

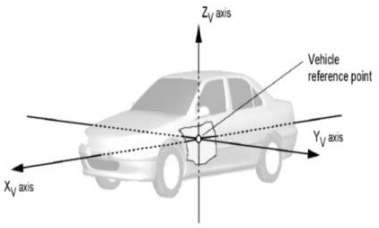

Fig.10. Coordinate system of the vehicle

The coordinate system should be established before the design of geometric parameters of suspension. Connect the two front wheel ground point and the midpoint of the line segment is set as the coordinate origin. Coordinate axis direction is shown in Figure.10.

The kingpin inclination angle is not conducive to the steering of vehicle, so it is set as 0 degrees. Then according to the scrub radius and the basic dimensions of the existing rims, tires and brake calipers, the coordinates of the external hard point of the upper and lower transverse arm in the Y axis and Z axis can be determined.

After determining the location of the external hard point of the transverse arm, it is necessary to determine the length of equivalent swing arm *fvsa* shown as equation (1). Considering comprehensively the influence of the change of the camber angle on the acceleration and braking performance of the vehicle, camber gain is taken as 0.5. Therefore, the *fvsa* length is equal to *t*. That is, the length of equivalent swing arm is equal to the front-wheel track. Then the location of the upper and lower transverse arm in straight line can be determined based on the location of the roll center.

$$fvsa = \frac{t}{2 \times (1 - camber\ gain)} \tag{1}$$

where *t* is the wheel track.

After determining the location of the straight line of the transverse arm, it is necessary to determine the transverse arm length. Generally, the length of the upper transverse arm is shorter than that of the lower transverse arm. According to the requirement of the competition for the driver's leg space that the internal frame must accommodate a square plate with the side length of 350mm, the coordinates of the internal hard point of the transverse arm in the Y axis and Z axis can be determined.

The caster angle and pneumatic trail of the front suspension have been determined, then the coordinates of the outer hard point of the suspension in the X axis can be obtained. The coordinates of the internal hard point of the suspension in the X axis need to be determined based on the general layout of the vehicle. Finally, the coordinates of the hard points of the front suspension transvers arm can be determined shown in Table 2.

Table 2. The coordinates of the hard points of the front suspension transverse arm

The hard points of transverse arm	X	Y	Z
The external hard point of the upper-left arm	-18.84	564	365.636
The internal hard point of the upper-left arm (front)	135	260	258.757
The internal hard point of the upper-left arm (rear)	-187	260	258.757
The external hard point of the lower-left arm	-4.1	564	145.816
The internal hard point of the lower-left arm (front)	135	160	92.641
The internal hard point of the lower-left arm (rear)	-197	160	92.641
The external hard point of the upper-right arm	-18.84	-564	365.636
The internal hard point of the upper-right arm(front)	135	-260	258.757
The internal hard point of the upper-right arm(rear)	-187	-260	258.757
The external hard point of the lower-right arm	-4.1	-564	145.816
The internal hard point of the lower-right arm(front)	135	-160	92.641
The internal hard point of the lower-right arm(rear)	-197	-160	92.641

Just like the front suspension design, in the design

of the rear suspension geometric parameters, it is also necessary to determine the coordinates of the external and internal hard point of the transverse arms in the X axis, Y axis and Z axis. The difference is that the rear wheel does not undertake the steering function, therefore, the kingpin angle, the scrub radius and the pneumatic trail can be usually determined based on the general layout of the vehicle. The coordinates of hard points of rear suspension transverse arm can be determined shown in Table 3.

Table 3. Hard points parameters of rear suspension arm

The hard points of the rear suspension	X	Y	Z
The external hard point of the upper-left arm	-1545	543.52	386.1
The internal hard point of the upper-left arm (front)	-1290	272.87	297.7
The internal hard point of the upper-left arm (rear)	-1555	272.87	297.7
The external hard point of the lower-left arm	-1570	543.52	126.8
The internal hard point of the lower-left arm (front)	-1350	166.16	92.9
The internal hard point of the lower-left arm (rear)	-1555	166.16	92.9
The external hard point of the upper-right arm	-1545	-543.52	386.1
The internal hard point of the upper-right arm(front)	-1290	-272.87	297.7
The internal hard point of the upper-right arm(rear)	-1555	-272.87	297.7
The external hard point of the lower-right arm	-1570	-543.52	126.8
The internal hard point of the lower-right arm(front)	-1350	-166.16	92.9
The internal hard point of the lower-right arm(rear)	-1555	-166.16	92.9

ELASTIC AND DAMPING ELEMENTS

The ground has an impact on the wheels when the vehicle is running, so it is necessary to add some elastic elements between the wheels and the body to form the elastic coupling. However, the elastic system subjected to the impact would vibrate continuously in a certain period, so it is also necessary to add some damping elements between the wheel and the body to attenuate vibration.

Layout Scheme

For the vehicle, the wheels and the spring shock absorber are generally connected by the connecting rod and the rocker arm. As shown in Figure.11, the left side is the push-rod arrangement, and the right side is the pull-rod arrangement. Considering the layout factors and the suspension performance, the pull-rod arrangement is used in the front suspension, and the push-rod arrangement is used in the rear suspension.

The transfer ratio, that is, the ratio of the beating displacement of the wheels and the deformation of the elastic elements, is determined by the geometric size of the rocker arm. Generally, the greater the transfer ratio, the smaller the geometric size of the rocker arm, the smaller the deformation of the elastic elements corresponding to the beating displacement of the same wheel. Because of the compact front suspension space, the transfer ratio of the front suspension is set to 2.0. While the rear suspension space is sufficient, the transfer ratio of the rear suspension is set to 1.0 to decrease the force of each mechanism, simplify the calculation and idealize the change of the suspension parameters.

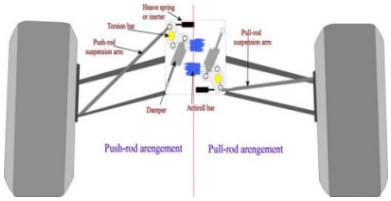

Fig. 11. Push-rod and pull-rod arrangement

Elastic Elements

Before the design of the elastic element, the related quality parameters of the vehicle should be determined, then the elastic element parameters can be determined based on the actual characteristic of the dynamic competition items. The required parameters for design are shown in Table 4.

The ride comfort stiffness refers to the series stiffness of the tire and the suspension when wheels of both sides are beating in the same direction. The mathematic relationship between the ride comfort stiffness and the offset frequency is shown as follows:

$$f = \frac{1}{2\pi}\sqrt{\frac{K}{M}} \tag{2}$$

$$K = 4\pi^2 f^2 M \tag{3}$$

where f is the offset frequency, K is the ride comfort stiffness, and M is the sprung mass.

In this paper, because the vehicle is not equipped with aerodynamic package and the offset frequency should not be too great, the offset frequency of the front suspension is set to 2.1Hz and that of the rear suspension is set to 1.9Hz. The symbols for each parameter in the calculation are shown in Table 5.

Table 4. The related quality parameters of the vehicle

Item	Front	Rear
Curb weight(including a 60kg driver)	125kg	125kg
Unsprung mass	25kg	25kg
Sprung mass	100kg	100kg
The height of gravity center	250mm	
The height of roll center	0mm	25.4mm
Effective radius of the tire	266.7mm	
Wheel base	1575mm	
Wheel track	1210mm	1117mm
Spring transfer ratio	2.0	1.0
Transfer ratio of anti-roll bar	0.15	0.1
Tire stiffness	116N/mm	111N/mm

First, the ride comfort stiffness of the front wheel frame can be calculated based on the offset frequency and the unsprung mass as follows:

$$K_{RF} = 4\pi^2\omega_F^2(W_{SF}/2) = 4\times\pi^2\times 2.1^2\times(100/2) = 8705N/m$$

Because the ride comfort stiffness is obtained by the tire stiffness and the suspension line stiffness in series, the suspension line stiffness can be calculated as follows:

$$K_{WF} = \frac{K_{RF} \cdot K_{TF}}{K_{TF} - K_{RF}} = \frac{8705 \times 116000}{116000 - 8705} = 9411N / m$$

After the suspension line stiffness is obtained, the spiral spring stiffness of the front suspension can be calculated based on the spring transfer ratio as follows:

$$K_{SF} = K_{WF} \cdot LR_F^2 = 9411 \times 2.0^2 = 37644N / m = 382.2lbs / in$$

Table 5. The symbols for each parameter

Item	Front		Rear
Curb weight (including a 60kg driver)	W_F		W_R
Unsprung mass	W_{UF}		W_{UR}
Sprung mass	W_{SF}		W_{SR}
The height of gravity center		h	
The height of roll center	Z_F		Z_R
Effective radius of the tire		RL	
Wheel base		l	
Wheel track	T_F		T_R
Spring transfer ratio	LR_F		LR_R
Transfer ratio of the anti-roll bar	LB_F		LB_R
Tire stiffness(tire pressure:69kPa)	K_{TF}		K_{TR}
Offset frequency	ω_F		ω_R
Ride comfort stiffness	K_{RF}		K_{RR}
Suspension line stiffness	K_{WF}		K_{WR}
Spring stiffness	K_{SF}		K_{SR}
Centroid height of the sprung mass		h_S	
Rolling arm length		h_{RM}	
Rolling moment		M_ϕ	
Lateral acceleration		A_y	
Rolling gradient		RG	
Rolling angle stiffness		K_ϕ	
Rolling angle stiffness generated by spiral spring	$K_{\phi SF}$		$K_{\phi SR}$
Rolling angle stiffness generated by anti-roll bar	$K_{\phi BF}$		$K_{\phi BR}$
Transfer load on the left and right		TLT	
The proportion of transfer load of the front and rear wheels		T_{ave}	

For the rear suspension, the ride comfort stiffness, the suspension line stiffness and the spiral spring stiffness can be calculated in the same method as follows:

$$K_{RR} = 4\pi^2 \omega_R^2 (W_{SR} / 2) = 4 \times \pi^2 \times 1.9^2 \times (100 / 2) = 7126N / m$$

$$K_{WR} = \frac{K_{RR} \cdot K_{TR}}{K_{TR} - K_{RR}} = \frac{7126 \times 111000}{111000 - 7126} = 7615N / m$$

$$K_{SR} = K_{WR} \cdot LR_R^2 = 7615 \times 1.0^2 = 7615N / m = 121lbs / in$$

In this paper, the rolling gradient is used as the evaluation index of the rolling angel stiffness of the vehicle. Because of the little downforce, smooth circuit and good road conditions, the rolling gradient is set to 1.5deg/g.

According to the centroid height of the vehicle and the unsprung mass, the centroid height of the spring mass, the load distribution of the sprung mass, and the vertical height from the rolling axis to the sprung mass centroid can be calculated as follows:

$$h_s = \frac{(W_F + W_R) \cdot h - W_{UF} \cdot RL - W_{UR} \cdot RL}{W_{SF} + W_{SR}} = \frac{250 \times 0.25 - (25 + 25) \times 0.2667}{200} = 0.2458m$$

$$a_S = \frac{W_{SF}}{W_{SF} + W_{SR}} \times 100\% = \frac{100}{200} \times 100\% = 50\%$$

$$h_{RM} = h_S - \left[Z_F + (Z_R - Z_F)(1 - a_S) \right] = 0.2458 - \left[0 + (0.0254 - 0) \times (1 - 50\%) \right] = 0.2331m$$

Then the relationship between the rolling moment and the lateral acceleration can be determined as follows:

$$\frac{M_\phi}{A_y} = (W_{SF} + W_{SR}) \cdot g \cdot h_{RM} = 200 \times 9.8 \times 0.2331 = 456.9N \cdot m / g$$

According to the identified rolling gradient and ride comfort stiffness, the rolling angle stiffness of the vehicle and the rolling angle stiffness generated by spiral spring can be calculated as follows:

$$K_\phi = \frac{M_\phi}{A_y} \cdot \frac{1}{RG} = \frac{456.9}{1.5} = 305N \cdot m / \deg$$

$$K_{\phi SF} = \frac{\pi}{360} K_{RF} \cdot T_F^2 = \frac{\pi}{360} \times 8705 \times 1.21^2 = 111.2N \cdot m / \deg$$

$$K_{\phi SR} = \frac{\pi}{360} K_{RR} \cdot T_R^2 = \frac{\pi}{360} \times 7126 \times 1.117^2 = 77.6N \cdot m / \deg$$

Then, the rolling angle stiffness of the anti-roll bar can be calculated as follows:

$$K_{\phi BF} + K_{\phi BR} = K_\phi - \left(K_{\phi SF} + K_{\phi SR} \right) = 305 - 188.8 = 116.2N \cdot m / \deg$$

When the vehicle is subjected to the lateral force, the transfer load on the left and right can be calculated as follows:

$$\frac{TLT}{A_y} = \frac{W_T \cdot g \cdot h}{T_{ave}} = \frac{250 \times 0.25 \times 9.8}{(T_F + T_R) / 2} = 526.3N / g$$

The lateral performance of the rear wheel is superior to that of the front wheel, and the distributed load of the front and rear wheels are equal, which causes the under-steering of the vehicle but more stable acceleration and steering. First, the rolling angle stiffness of the front wheel can be calculated as follows:

$$\frac{1}{2} \cdot \frac{TLT}{A_y} = \frac{\phi \cdot K_{\phi F}}{T_F} + \frac{W_{SF} \cdot g \cdot Z_F}{T_F} + \frac{W_{UF} \cdot RL_F}{T_F} = \frac{1.5K_{\phi F}}{1.21} + \frac{100 \times 9.8 \times 0}{1.21} + \frac{25 \times 0.2667 \times 9.8}{1.21}$$

$$K_{\phi F} = 168.7N \cdot m / \deg$$

The sum of the rolling wheel stiffness generated by the front anti-roll bar and the front suspension spiral spring is equal to the rolling wheel stiffness of the front wheel, so the rolling angle stiffness generated by the front and rear anti-roll bars can be calculated as follows:

$$K_{\phi BF} = K_{\phi F} - K_{\phi SF} = 168.7 - 111.2 = 57.5N \cdot m / \deg$$

$$K_{\phi BR} = K_\phi - K_{\phi F} - K_{\phi SR} = 305 - 168.7 - 77.6 = 58.7N \cdot m / \deg$$

Damping Elements

The damping ratio is used to characterize the damping of the damping elements, and it refers to the ratio of the damping coefficient and the critical damping. The relationship among the critical damping, the sprung mass and the suspension line stiffness is shown as follows:

$$C_{CR} = 2\sqrt{K_S W_s} \qquad (4)$$

where C_{CR} is the critical damping, K_S is the suspension line stiffness and W_S is the sprung mass.

Generally, the damping ratio ranges from 0.65 to 0.7 to provide sufficient support and reduce overshoot. Therefore, the original damping ratio is set to 0.7. The damping coefficient of the front and rear suspension can be calculated as follows:

$$C_F = \zeta \cdot C_{CR} = 2\zeta \sqrt{K_{SF} \cdot W_{SF}} = 2 \times 0.7 \times \sqrt{21175 \times 100} = 2037N / (m / s) = 2.037N / (mm / s)$$

$$C_R = \zeta \cdot C_{CR} = 2\zeta \sqrt{K_{SR} \cdot W_{SR}} = 2 \times 0.7 \times \sqrt{7615 \times 100} = 1222N / (m / s) = 1.222N / (mm / s)$$

Because the shock absorber is connected with the spiral spring in parallel and transmits the force by the rocker arm, the damping coefficient of the shock absorber can be calculated as follows:

$$C_{DamF} = C_F \cdot LR_F^2 = 2.037 \times 2.0^2 = 8.148N/(mm/s)$$
$$C_{DamR} = C_R \cdot LR_R^2 = 1.222 \times 1.0^2 = 1.222N/(mm/s)$$

where C_{DamF} and C_{DamR} are the damping coefficient of the shock absorber of the front and rear suspension.

To improve the performance of the vehicle chassis, the four channel adjustable shock absorber is chosen for the vehicle, which contains four valves-the compression and rebound valves at low speed side and the compression and rebound valves at high speed side. The damping coefficient of the compression and rebound valves at low speed side are two-thirds and one and half of the original damping coefficient respectively, and the damping coefficient of the valves at high speed side is half of that of the valves at low speed side.

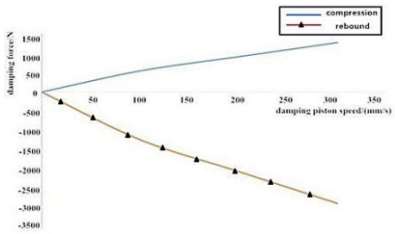

Fig. 12. The ideal damping characteristic curve

Finally, the ideal damping characteristic curve can be obtained shown in Figure. 12. The horizontal axis represents the damping piston speed (mm/s) and the vertical axis represents the damping force (N).

The SUSPENSION SYSTEM ANALYSIS

The Establishment of Suspension System Model

In this paper, the kinematic simulation of the suspension system is carried out based on Optimum K software. First, the suspension type is defined, then the coordinates of the hard points and the simulation conditions are input to start the simulation analysis.
The dynamic simulation of the suspension system is carried out based on Adams Car software. Firstly, each subsystem template is established according to the properties file, then the subsystem is built based on the established template, finally the subsystems are assembled into components and added to the test-bed.

The dynamic model of the vehicle suspension system is shown in Figure.13.

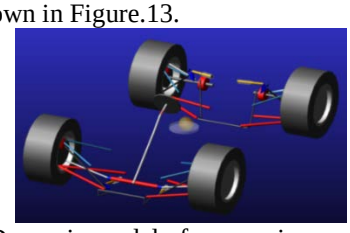

Fig.13. Dynamic model of suspension system

Kinematic Analysis of Suspension System

Vertical jitter condition

Generally, the suspension stroke is at least 25.4mm, so the beating displacement of the vehicle under the vertical heave condition is set to 25.4mm.

The curves of camber angle with the change of vehicle body displacement are shown in Figure.14. The horizontal axis represents the vertical displacement of the body, and the initial displacement is 0mm. As can be seen from Fig.14, when the body displacement ranges from -25.4mm to 25.4mm, the front wheel camber angle ranges from -1.4deg to 1.1deg and the rear wheel camber angle ranges from -1.4deg to 1.2deg, which are in reasonable range.

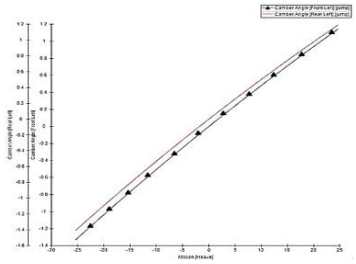

Fig.14. Camber angle under vertical heave condition

The curves of toe angle with the change of vehicle body displacement are shown in Figure.15 (the two curves coincide). When the body displacement ranges from -25.4mm to 25.4mm, the toe angle ranges from 0.3deg to -0.15deg. When braking, the vertical load of the vehicle transfers to the front wheel, the body generates pitching movement (braking nod) and the toe angle increases, which causes the over-steering of the vehicle but is conducive to the vehicle into the bend.

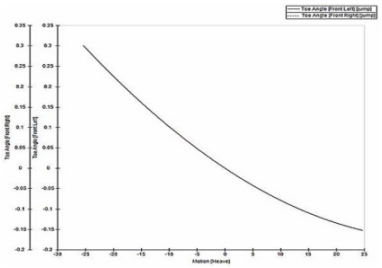

Fig.15. Toe angle under vertical heave condition

When accelerating, the vertical load of the vehicle transfers to the rear wheel, the body also generates pitching movement (squatting) and the toe angle decreases, which maintains the stability of accelerating out of the bend.

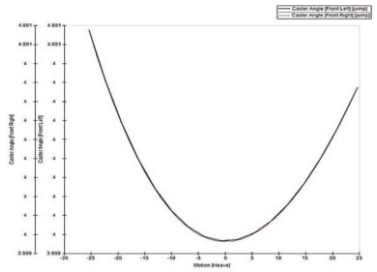

Fig.16. Kingpin caster angle under vertical heave condition

The curves of kingpin caster angle of the front wheel with the change of vehicle body displacement are shown in Figure.16 (the two curves coincide). The value of the kingpin caster angle would have an effect on the pneumatic trail, thereby affecting the feedback force of the steering wheel to the steering wheel, so its change should be as small as possible. As can be seen from Fig.16, when the body displacement ranges from -25.4mm to 25.4mm, the kingpin caster angle ranges from 4.001deg to 3.999deg and the variation can be ignored.

Rolling condition

The curve of the camber angle with the change of the rolling angle is shown in Figure.17. The initial rolling angle of the body is 0deg. When the rolling angle ranges from -2deg to 2deg, the camber angles of the front and rear wheel range from 0.9deg to -1deg and the camber gain is 0,5, which meets the design requirement.

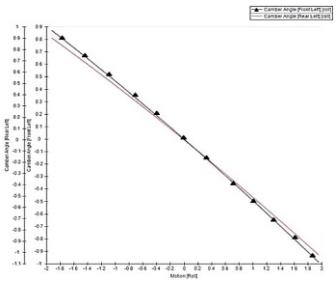

Fig.17. Camber angle under rolling condition

The curves of roll center height with the change of rolling angle are shown in Figure.18. As can be seen from Fig.18, when the rolling angle ranges from -2deg to 2deg, for the roll center height of the front suspension, the difference between the maximum and the minimum is 3.4mm, and for the roll center height of the rear suspension, the difference between the maximum and the minimum is 0.19mm. The differences meet the design requirement.

The curves of toe angle with the change of rolling angle are shown in Figure.19. The initial rolling angle and toe angle are 0deg. As can be seen from Fig.19, when the vehicle turns left and rolls to the right, the rolling angle is greater than 0deg, the toe angle of the right wheel increases and the toe angle of the left wheel decreases, which is conducive to the steering stability. And the difference between the maximum and the minimum of the toe angle is 0.38deg, which meets the design requirement.

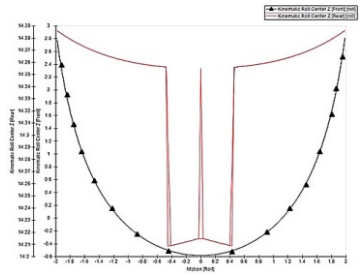

Fig.18. Roll center height under rolling condition

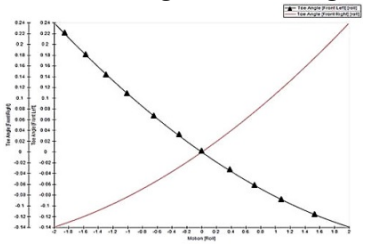

Fig.19. Toe angle under rolling condition

Dynamic Analysis of Suspension System

Accelerating condition

The curve of pitching angle with the change of longitudinal acceleration is shown in Figure.20. The horizontal axis represents the longitudinal acceleration and the vertical axis represents the pitching angle of the body. As can be seen from Fig.20, the initial pitching angle is -0.766deg, when the longitudinal acceleration ranges from 0g to 0.7g, the pitching angle increases by 1.46deg, which meets the design requirement.

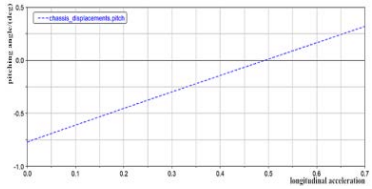

Fig.20. Pitching angle under accelerating condition

The curves of spiral spring deformation with the change of longitudinal acceleration are shown in Fig.21. As can be seen from Figure.21, when the longitudinal acceleration ranges from 0g to 0.7g, the spiral spring of the front suspension is stretched by 6mm, and the spiral spring of the rear suspension is compressed by 17mm. According to the transfer ratio of the elastic element, it can be inferred that compared to the body, the beating value of the front wheel is 12mm and the beating value of the rear wheel is 17mm.

The curves of camber angle with the change of longitudinal acceleration are shown in Figure.22. As can be seen from Fig.22, when the longitudinal acceleration ranges from 0g to 0.7g, the camber angle of the front wheel increases by 0.66deg and the camber angle of the rear wheel decreases by 0.97deg, which is in the reasonable range.

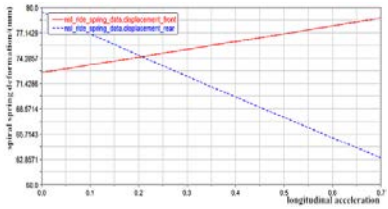

Fig.21. Spiral spring deformation under accelerating

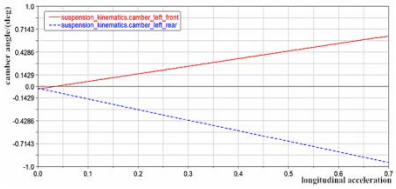

Fig.22. Camber angle under accelerating condition

Braking condition

The curve of pitching angle with the change of longitudinal acceleration is shown in Figure.23. The horizontal axis represents the longitudinal acceleration and the vertical axis represents the pitching angle of the body. As can be seen from Fig.23, the initial pitching angle is -0.766deg, when the longitudinal acceleration ranges from 0g to -0.98g, the pitching angle decreases by 1.42deg, which meets the design requirement.

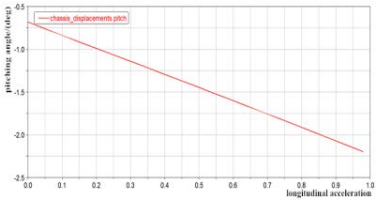

Fig.23. Pitching angle under braking condition

The curve of the spiral spring deformation with the change of the longitudinal acceleration is shown in Figure.24. As can be seen from Fig.24, when the longitudinal acceleration ranges from 0g to -0.98g, the spiral spring of the front suspension is compressed by 7.25mm, and the spiral spring of the rear suspension is stretched by 24.82mm. According to the transfer ratio of the elastic element, it can be inferred that compared to the body, the beating value of the front wheel is 14.5mm and the beating value of the rear wheel is 25mm.

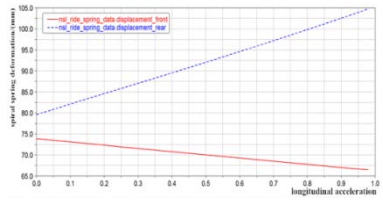

Fig.24. Spiral spring deformation under braking

The curve of the camber angle with the change of the longitudinal acceleration is shown in Figure.25. As can be seen from Fig.25, when the longitudinal acceleration ranges from 0g to -0.98g, the camber angle of the front wheel decreases by 0.88deg and the camber angle of the rear wheel increases by 1.26deg, which is in the reasonable range.

Steering condition

The curve of the rolling angle with the change of the lateral acceleration is shown in Figure.26. The horizontal axis represents the lateral acceleration and the vertical axis represents the rolling angle of the body. As can be seen from Fig.26, the initial rolling angle is 0deg, when the lateral acceleration ranges from 0g to -0.98g, the rolling angle increases by 1.5deg and the rolling gradient is 1.5deg/g, which meets the design requirement.

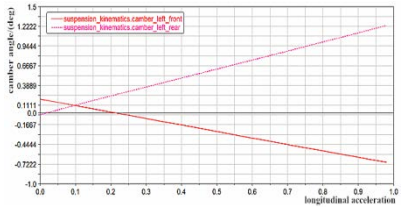

Fig.25. Camber angle under braking condition

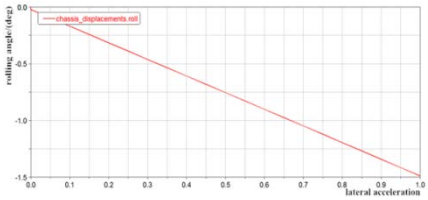

Fig.26. Rolling angle under steering condition

The curve of the vertical load with the change of the lateral acceleration is shown in Figure.27. As can be seen from Fig.27, when the lateral acceleration ranges from 0g to 0.98g, the vertical load of the left-front wheel increases from 595.6N to 899.2N and the vertical load of the left-rear wheel increases from 627N to 837.7N, the total transfer load is 514.3N, which is basically consistent with the checking result.

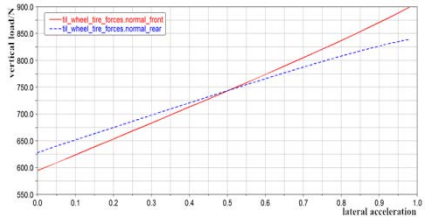

Fig. 27. Wheel vertical load under steering condition

CONCLUSIONS

In this paper, the suspension system of vehicle is taken as the research object. And the design and analysis of suspension system have been discussed based on tire characteristics. According to the tire characteristics and the vehicle related quality parameters, the geometric parameters of suspension transverse arm, the stiffness of elastic element and the

ideal damping characteristic curve of damping element are determined. The kinematic and dynamic models of the vehicle suspension system are established. The kinematic and dynamic analysis of the suspension system are carried out, and the results show that the suspension system design achieves the design goal.

ACKNOWLEDGMENT

This work is supported by the National Natural Science Foundation of China (51675324), the key project of Shanghai Science and Technology Commission (15110501100).

REFERENCES

Angrosch, B., Plöchl, M. and Reinalter, W., "Suspension design by means of numerical sensitivity analysis and optimization," International Journal of Vehicle Design, Vol. 65, No. 1, pp. 52-72.(2014).

Balamurugan, L., Jancirani, J. and Eltantawie, M.A., "Generalized magnetorheological (MR)damper model and its application in semi-active control of vehicle suspension system," International Journal of Automotive Technology, Vol. 15, No. 3, pp. 419-427. (2014).

Eskandary, P.K., Khajepour, A., Wong, A. and Ansari, M., "Analysis and optimization of air suspension system with independent height and stiffness tuning," International Journal of Automotive Technology, Vol. 17, No. 5, pp. 807-816. (2016).

Hurel, J., Mandow, A. and Garcia, A., "Kinematic and dynamic analysis of the McPherson suspension with a planar quarter-car model," Vehicle System Dynamics, Vol. 51, No. 9, pp.1422-1437. (2013).

Jamali, A., Shams, H. and Fasihozaman, M., "Pareto multi-objective optimum design of vehicle suspension system under random road excitations," Proceedings of the Institution of Mechanical Engineers, Part K: Journal of Multi-body Dynamics, Vol. 228, No. 3, pp. 282-293. (2014).

Kang, D.O., Heo, S.J. and Kim, M.S., "Robust design optimization of the McPherson suspension system with consideration of a bush compliance uncertainty," Proceedings of the Institution of Mechanical Engineers, Part D: Journal of Automobile Engineering, Vol. 224, No. 6, pp.705-716. (2010).

Kim, G., Kang, S., Lee, Y., Park, S. and Jung, W., "Study on durability and reliability of strut type suspension noise based on experimental methods," Journal of Mechanical Science and Technology, Vol. 26, No. 1, pp. 21-29. (2012).

Liu, X.T., Wang, M.L., Wang, X.L., Li, C.C. and Guo H., "Hardpoint correlation analysis and optimal design for front suspension of a Formula SAE car," Australian Journal of Mechanical Engineering, Vol. 13, No. 2, pp. 67-76. (2015).

Mastinu, G., Gobbi, M. and Miano, C., "Optimal design of complex mechanical systems," Berlin: Springer Berlin Heidelberg. (2006).

Pacejka, H.B., "Tire and vehicle dynamics," Butterworth-Heinemann. (2002).

Park, S.J. and Sohn, J.H., "Effects of camber angle control of front suspension on vehicle dynamic behaviors," Journal of Mechanical Science and Technology, Vol. 26, No. 2, pp. 307-313. (2012).

Reimpell, J., Stoll, H. and Betzler, J., "The automotive chassis: engineering principles," Warrendale, PA: Society of Automotive Engineers International. (2001).

Stéphant, J., Charara, A. and Meizel, D., "Evaluation of a sliding mode observer for vehicle side-slip angle," Control Engineering Practice, Vol. 15, No. 7, pp. 803-812. (2007).

Uchida, T. and Mcphee, J., "Driving simulator with double-wishbone suspension using efficient block-triangularized kinematic equations," Multi-body System Dynamics, Vol. 28, No. 4, pp. 331-347. (2012).

Wolfgang, M., "Road vehicle suspension," New York: John Wiley & Sons, Inc. (1998).

基於輪胎特性的懸架系統設計與分析

梁誌強 劉新田 左賀 王岩松

上海工程技術大學

摘要

懸架系統是影響汽車乘坐舒適性和穩定性的關鍵零部件。本文研究了如何設計並分析懸架系統。首先，基於輪胎特性，確定了懸架橫臂、彈性元件和阻尼元件的幾何參數。其次，建立了車輛懸架系統的動力學模型。最後進行了運動學和動力學分析，來验证懸架系統設計的有效性。分析結果顯示，本文提出的懸架系統設計方法具有一定的有效性。